Title

Coordination of contractility, adhesion and flow in migrating Physarum amoebae

Journal

Journal of The Royal Society Interface, 12(106)

ISSN

1742-5689

Authors

Lewis, Owen L
Zhang, Shun
Guy, Robert D
et al.

Publication Date

2015-05-01

DOI

10.1098/rsif.2014.1359

Peer reviewed

INTERFACE

rsif.royalsocietypublishing.org

Research

Cite this article: Lewis OL, Zhang S, Guy RD, del Álamo JC. 2015 Coordination of contractility, adhesion and flow in migrating *Physarum* amoebae. *J. R. Soc. Interface* **12**: 20141359.
http://dx.doi.org/10.1098/rsif.2014.1359

Received: 11 December 2014
Accepted: 1 April 2015

Subject Areas:
biomathematics

Keywords:
amoeboid motility, traction force microscopy, cytoplasmic streaming, cell locomotion, particle image velocimetry

Author for correspondence:
Owen L. Lewis
e-mail: olewis@math.utah.edu

Electronic supplementary material is available at http://dx.doi.org/10.1098/rsif.2014.1359 or via http://rsif.royalsocietypublishing.org.

THE ROYAL SOCIETY PUBLISHING

Coordination of contractility, adhesion and flow in migrating *Physarum* amoebae

Owen L. Lewis[1], Shun Zhang[2], Robert D. Guy[3] and Juan C. del Álamo[2]

[1]Department of Mathematics, University of Utah, Salt Lake City, UT, USA
[2]Mechanical and Aerospace Engineering Department, University of California San Diego, La Jolla, CA, USA
[3]Department of Mathematics, University of California Davis, Davis, CA, USA

This work examines the relationship between spatio-temporal coordination of intracellular flow and traction stress and the speed of amoeboid locomotion of microplasmodia of *Physarum polycephalum*. We simultaneously perform particle image velocimetry and traction stress microscopy to measure the velocity of cytoplasmic flow and the stresses applied to the substrate by migrating *Physarum* microamoebae. In parallel, we develop a mathematical model of a motile cell which includes forces from the viscous cytosol, a poro-elastic, contractile cytoskeleton and adhesive interactions with the substrate. Our experiments show that flow and traction stress exhibit back-to-front-directed waves with a distinct phase difference. The model demonstrates that the direction and speed of locomotion are determined by this coordination between contraction, flow and adhesion. Using the model, we identify forms of coordination that generate model predictions consistent with experiments. We demonstrate that this coordination produces near optimal migration speed and is insensitive to heterogeneity in substrate adhesiveness. While it is generally thought that amoeboid motility is robust to changes in extracellular geometry and the nature of extracellular adhesion, our results demonstrate that coordination of adhesive forces is essential to producing robust migration.

1. Introduction

Cell migration plays a critical role in a wide variety of biological processes, including morphogenesis, wound healing and the immune response. Amoeboid motility is a fast type of cell migration defined by large shape changes as the cell extends and retracts various pseudopodia and blebs [1]. These extensions are driven by the interplay between substrate adhesion, the polymerization of filamentous actin and the pressure-driven flow of cytoplasm [2]. Research on amoeboid motility has recently intensified in part because this migration mode is robust to changes in the extracellular matrix and because of the specific molecular nature of the cell–matrix adhesions [3,4]. That is to say, amoeboid cells are able to cross barriers, move through confined channels or squeeze through three-dimensional matrices by contracting and pushing-off the surrounding environment. This versatility has also spurred the exploratory design of bioinspired millimetric robots made of active self-oscillating hydrogels [5]. Despite the vast existing knowledge about the biological and molecular processes involved in cell migration, our understanding of the underlying mechanical processes is still rather phenomenological. In particular, the coordination of contractility, adhesion and flow of cytoplasmic material that enables pseudopod extension is not fully understood. In fact, it is not even clear if coordination of these processes is necessary for motility in all scenarios [3].

This work investigates the coordination of cellular contractile force, substrate adhesion and cytoplasmic flow in migrating amoebae of the slime mould *Physarum polycephalum*. *Physarum* plasmodia generate a periodic flow of cytoplasm (known as shuttle streaming) through a tubular network. This flow is driven by pressure gradients created by contraction of the actomyosin network within the plasmodium [6–8]. Small-scale *Physarum* amoebae (approx. 100 µm in length) can exhibit a similar behaviour where a rhythmic flow of cytoplasm moves back and forth along the centreline of a roughly tadpole-shaped cell. The onset of this behaviour has been observed to coincide with a drastic increase in

the locomotion speed of growing *Physarum* [9]. Larger scale plasmodia ($l \sim 500$ μm) can develop more complex morphologies including chains of round contractile heads connected by relatively inert tubes, as shown by Rieu *et al.* in a companion paper [10].

Owing to the relatively large scale of the organism, particle image velocimetry (PIV, [11]) experiments allow researchers to measure the intracellular fluid velocity in *Physarum* amoebae using cell organelles as flow tracers. The periodic waves of cytoplasmic streaming in tadpole-shaped cells have been well characterized by PIV, and it has been argued that the travelling wave nature of the intracellular flow is responsible for generating directed motility [12]. However, a purely hydrodynamic explanation of *Physarum* amoeboid motility does not address the transmission of traction stress to the underlying substrate, which is ultimately necessary for cellular migration to take place. It is unclear if passive, uncoordinated cell–substrate interactions are sufficient for *Physarum* plasmodia to effectively 'flow' across a substrate. Alternately, the motility of *Physarum* plasmodium might depend upon cell–substrate adhesion being dynamically coordinated relative to the stresses generated by the flow. It is known that substrate-bound structures are mechanically linked to the actomysosin network within the plasmodium [13]. However, the precise nature of these structures is not well studied, and there currently exists no quantitative description of the stresses which the cell exerts on the substrate as it migrates, nor how these stresses are correlated to the cytoplasmic flow.

To answer these questions, we concurrently perform traction force microscopy (TFM) and PIV measurements on migrating *Physarum* amoebae. In the past, TFM has been used to study the adhesive forces that enact locomotion of a diverse array of unicellular and multicellular organisms ranging from a few micrometres to a few centimetres in size [14–17]. In conjunction with these experiments, we develop a computational model for migrating *Physarum* amoebae based on a modified immersed boundary (IB) method [18]. The model accounts for hydrodynamic effects, elastic forces within the cell interior, and adhesive coupling of the cytoskeleton to the substrate. We use the model to examine how cytoskeletal contraction, cyotosolic flow, and cell–substrate adhesion work together to generate cell locomotion.

Our measurements show that traction stresses in migrating *Physarum* amoebae are mainly distributed along the cell periphery forming an inward contractile pattern. These stresses are spatio-temporally modulated to establish a rhythmic contraction wave that travels in the direction of cell migration. The contractile wave has the same time period as the intracellular flow waves previously described, and a phase lag of approximately one-third of a cycle. These spatio-temporal flow and stress patterns are reproduced by the numerical simulations using an idealized model of adhesion. We apply this adhesion model to investigate the strength of adhesion and its coordination *relative* to the rhythmic flow of cytoplasm. Specific coordination patterns are identified which are consistent with experimental data. These parameters are seen to be optimal in that they (nearly) maximize migration velocity of the model cell for a given strength of actomyosin contraction. Finally, we perform numerical simulations of the model cell crawling across randomly heterogeneous substrates and show that the speed of migration is only mildly perturbed. These simulations imply that the proposed model of motility is robust to perturbations of adhesiveness of the extracellular substrate.

2. Experimental material and methods

This section summarizes the cell culture, microscopy and analysis methods employed to prepare migrating *Physarum* microamoebae, and to jointly measure the intracellular flows and traction forces generated by these amoebae while migrating. A more exhaustive description of these methods can be found in the electronic supplementary material. *Physarum* plasmodia were obtained from a generous gift by Toshiyuki Nakagaki (Research Institute for Electronic Science, Hokkaido University, Japan) and cultured as previously described [12]. Small portions of area around 0.2×0.2 mm^2 were cut from the parent plasmodia to produce migrating amoebae, which were transferred to collagen-coated polyacrylamide (PA) gels embedded with fluorescent beads. The PA gels were prepared as previously described [19]. We kept the PA gel humidified throughout the experiment and flattened the amoebae to facilitate intracellular flow visualization by placing an agarose cap on top of the PA gel containing the specimen.

Using an inverted microscope, we simultaneously acquired transmitted light and fluorescence *z*-stack image sequences of the migrating *Physarum* amoebae with time resolutions of 0.2 s and 12 s, respectively. These data enabled us to jointly measure the intracellular flow and traction forces generated by the amoebae, which oscillate with a much slower period of approximately 100 s [12].

Physarum's dense distribution of intracellular vesicles was exploited to determine intracellular streaming velocities from the transmitted light images using PIV [11,12]. The raw image sequences were pre-processed for PIV by applying high-pass, band-pass and low-pass temporal filters, which allowed us to resolve the flow inside narrow channels (§4.1). The resulting spatial resolution of the flow measurements was 6.5 μm.

The three-dimensional deformation produced by *Physarum* amoebae on the PA substrate was measured by tracking the displacements of the embedded fluorescent beads as described by del Álamo *et al.* [19]. From the measured deformation, we computed the traction stresses (§4.2) and strain energy (§4.5) generated by the cells using Fourier TFM methods described elsewhere [16,19]. The spatial resolution of these measurements was 13 μm.

3. Mathematical model

Our model of the cell incorporates the effects of intracellular liquid (cytosol), the solid internal cell structure (cytoskeleton) and interaction with the extracellular substrate (through adhesion) in a moving geometry defined by the cell membrane and underlying cortex (figure 1). The model is described by the balance of forces on three materials: the liquid cytosol, the porous elastic cytoskeleton and the adhesive complexes which mechanically couple the cell interior to the substrate. The velocity of the viscous cytosol ($\boldsymbol{u}_f$) satisfies the forced Stokes equations. The fluid forces (viscosity and pressure) are balanced by body forces from the drag due to the internal cytoskeleton ($\boldsymbol{f}_{\mathrm{drag}}$) and the elastic forces on the membrane/cortex which bounds the cell ($\boldsymbol{f}_{\mathrm{mem}}$). The forces acting on the cytoskeleton are the elastic forces due to deformation ($\boldsymbol{F}_{\mathrm{e}}$), an active contractile force due to myosin molecular motors in the actin network ($\boldsymbol{F}_{\mathrm{a}}$), drag due to the cytosol ($\boldsymbol{F}_{\mathrm{drag}}$), forces due to adhesions to the substrate ($\boldsymbol{F}_{\mathrm{adh}}$) and forces generated by attachment of the cytoskeletal network to the surrounding

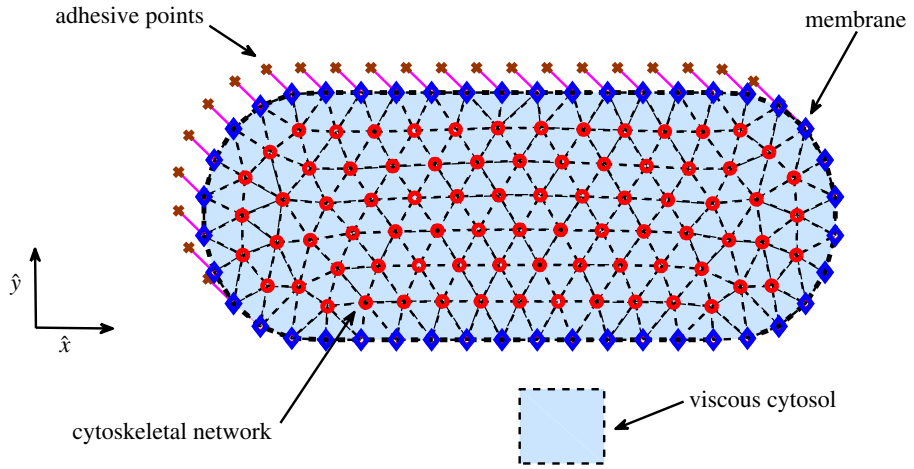

Figure 1. A schematic of our computational model of a *Physarum* plasmodium. Cytoskeletal network points are shown as circles. Membrane points are shown as diamonds. Adhesive points are illustrated as crosses. Viscous cytosol that permeates the porous media is illustrated as shading. (Online version in colour.)

membrane/cortex ($\boldsymbol{F}_{\text{net}}^{\text{attach}}$). Finally, the adhesion complexes are subject to forces applied by the external substrate ($\boldsymbol{F}_{\text{subs}}$), balanced by the forces which the complexes apply to the internal cytoskeleton. The system of equations which describe these force balances is

$$\mu\Delta\boldsymbol{u}_f - \nabla p + \boldsymbol{f}_{\text{drag}} + \boldsymbol{f}_{\text{memb}} = 0, \tag{3.1}$$

$$\nabla \cdot \boldsymbol{u}_f = 0, \tag{3.2}$$

$$\boldsymbol{F}_{\text{e}} + \boldsymbol{F}_{\text{a}} + \boldsymbol{F}_{\text{drag}} + \boldsymbol{F}_{\text{adh}} + \boldsymbol{F}_{\text{net}}^{\text{attach}} = 0 \tag{3.3}$$

and

$$\boldsymbol{F}_{\text{subs}} - \boldsymbol{F}_{\text{adh}} = 0. \tag{3.4}$$

These equations effectively describe the cell interior as an actively contractile poro-elastic network. A similar model (with an additional description of chemical kinetics) has been used to investigate symmetry breaking and the onset of contractile waves in *Physarum* microplasmodia [20,21]. For a description of how we compute these forces and the material parameters, see [22], as well as the electronic supplementary material, §S.2.

The active contractile force ($\boldsymbol{F}_{\text{a}}$) drives the deformation of the cell and the flow of cytosol. We assume that this force is generated by a travelling wave of isotropic contractile *stress* with magnitude

$$\Sigma_a(x, t) = \frac{C}{2}\left(\cos\left(\frac{2\pi}{\ell_{\text{cont}}}x - \frac{2\pi}{T}t\right) + 1\right), \tag{3.5}$$

where C is the maximum contractile stress, ℓ_{cont} is the wavelength and T is the period. The spatial variable x is the longitudinal body coordinate of the cell. The wave travels along the body (from posterior to anterior) with wavespeed ℓ_{cont}/T. We assume that the resulting wave of cell shape deformation is directly correlated with the underlying cytoskeletal contraction and choose $\ell_{\text{cont}} = 1600\ \mu\text{m}$ (four body lengths) and $T = 100$ s, which is consistent with the wavelength and period of deformation reported in [12] and with our own experiments. Similarly, the value of C is chosen so that the resulting deformations of the model cell are on the same scale as those observed in experiments.

Many of the material parameters can be measured or estimated. Conversely, the precise nature of the proteins with which *Physarum* adheres to the substrate is not known, even if some candidates have been identified [23]. The period of the deformations observed in *Physarum* is long (approx. 100 s) compared with the timescale of the dynamics of a cell–substrate bond, and so we represent the dynamics of adhesion via a viscous drag law [24] of the form

$$\boldsymbol{F}_{\text{subs}} = -\zeta(x, t)\boldsymbol{U}_{\text{adh}}, \tag{3.6}$$

where $\boldsymbol{U}_{\text{adh}}$ is the velocity of the adhesion complexes (relative to the substrate), and ζ is a viscous interaction coefficient. In §4.5, we investigate an idealized ζ of the form

$$\zeta(x, t) = \frac{A}{2}\left(\cos\left(\frac{2\pi}{\ell_{\text{adh}}}x - \frac{2\pi}{T}t + \phi\right) + 1\right) + \epsilon. \tag{3.7}$$

This choice of ζ is inspired by the observation that both the deformation of and associated flow within *Physarum* appear to propagate from the posterior to the anterior of the cell as a travelling wave (discussed in more detail in §4). The wavelength ℓ_{adh} and period T of the adhesion modulation are assumed to be the same as those of the contractile wave. The parameter ϕ represents the phase of the coordinated adhesion *relative* to the travelling wave of contraction strength (equation (3.1)). The amplitude parameter A is a measure of the strength of active coordinated adhesion, and will often be referred to as the 'coefficient of adhesion' in the following text. The parameter ϵ represents non-specific adhesive interactions between the substrate and the basal surface of the cell. We report the coefficient of adhesion in non-dimensional units of $[A/\epsilon]$.

4. Results

4.1. Cell behaviour

Upon reaching an adequate size (approx. 100 µm across), we observe that the cells elongate into a tadpole-like shape concurrent with the onset of a rhythmic, pulsating flow of cytosol. In most cases, this behaviour is similar to that reported in [12], with waves of contraction and flow travelling from posterior to anterior along the long axis of the cell. We refer to these cells as 'peristaltic'. We also observe a second mode of deformation which we call 'amphistaltic' due to the fact that the front and rear contract and relax in an anti-phase manner. The amphistaltic amoeboid mode could be the precursor of the contractile dumbbells found by Rieu *et al.* in the companion paper [10]. Of the 21 cells we study, 10 of them clearly exhibit the peristaltic behaviour, while six are amphistaltic. For an illustration of the difference between these modes, see the electronic supplementary

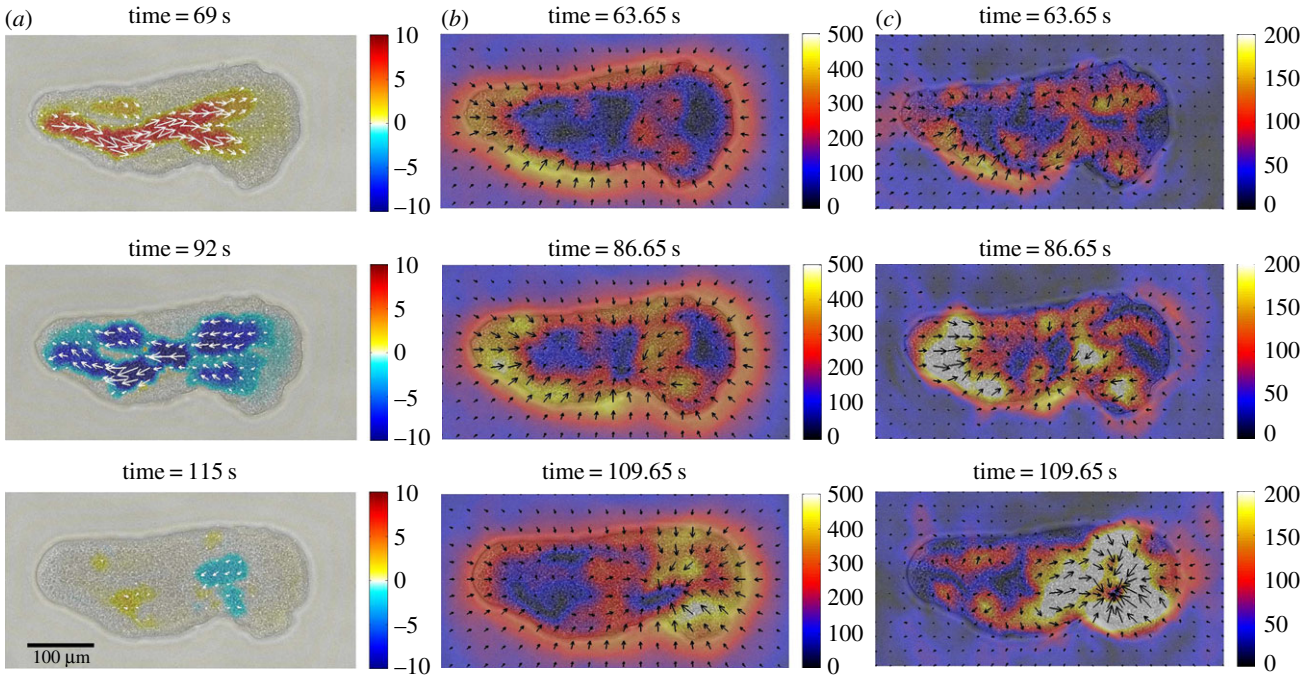

Figure 2. (*a*) Instantaneous intracellular flow observed in migrating *Physarum*. Arrows indicate the direction of flow; the colourmap indicates the projection of flow velocity onto the cell axis (μm s^{-1}). (*b*) Instantaneous traction stresses exerted on the substrate. Arrows indicate the direction of traction stress; the colourmap indicates the magnitude (Pa). (*c*) Traction stresses with the moving cortical average removed. Arrows indicate the direction of stresses; the colourmap indicates the magnitude (Pa). All arrow fields are downsampled by a factor of 4 in each direction for visual clarity. (Online version in colour.)

material. Approximately five of the cells we observe do not obviously fall into the category of peristaltic or amphistaltic mode and exhibit characteristics of each. The peristaltic mode appears to be stable on timescales of at least 1000 s. After this, the cells migrated far enough to leave the observation window. In this work, we focus only on the peristaltic cells due to the fact that they migrate approximately twice as fast as amphistaltic cells and are consistent with the experiments of previous investigations [12].

In peristaltic cells, the cytoplamsic flow is primarily directed along the cell centreline from its anterior to its posterior end (hereafter referred to as the longitudinal or cell axis) and has a distinct period of 90 ± 12 s (measured over 10 cells). A region of cytoplasmic flow directed forward develops at the cell rear. This pattern of forward flow becomes more prominent and travels along the cell axis towards the cell front. Eventually, a region of flow directed backwards emerges at the cell rear, and it also propagates towards the cell front, before the entire pattern repeats. Figure 2*a* shows three instantaneous measured velocity fields: a fully developed forward flow pattern, a fully developed backward-directed flow pattern, and the final stages of the backward flow pattern, as a new forward flow begins at the posterior of the cell. The emergence of this periodic wave of back-and-forth flow is observed to coincide with a dramatic increase in the migration velocity of the cell [9].

The migration of the cell is necessarily accompanied by the application of traction stresses to the substrate. Figure 2*b* shows a sequence of the stresses applied to the substrate by *Physarum* at three time points which are approximately those reported in figure 2*a*. There is a slight time difference between the images of (figure 2*a* and *b*) due to changing the imaging channel of the microscope from bright field to fluorescent field. The electronic supplementary material, movie 1, shows the joint time evolution of intracellular flow and traction stresses for the cell in figure 2.

The dominant feature of this traction stress pattern is purely contractile, with the larger stresses distributed along the cell periphery. This behaviour has been observed in other cell types, and it has been hypothesized that this effect is due to strong stresses associated with the cell cortex and directed out of the plane of the substrate [25]. Because our model only considers in-plane stress, we remove the average 'cortical' stress from the measured stress field to compare with model predictions (see the electronic supplementary material). At each instant of time, the average traction stress field is compiled from the traction stresses recorded during the previous, current and following periods of the observed behaviour. We then remove the average contractile stress from the instantaneous traction stress field, yielding the stress patterns shown in figure 2*c*. This procedure reveals loci of expansive and contractile stress that propagate from the posterior to the anterior. As the expansive locus leaves the front of the cell, a new one develops behind the contractile locus.

4.2. Comparison of model behaviour

In this section, we illustrate the behaviour of our model simulations and compare with experimental observations. All simulations were run with $\phi = 3\pi/2$ and $A = 100\epsilon$, respectively. In §4.4 and 4.5, we justify this choice and consider other adhesion parameters. In figure 3*a*, we show instantaneous fluid velocity fields obtained from the model at time intervals analogous to figure 2. The three panels illustrate a fully developed forward flow, a fully developed region of backward flow and the onset of a forward flow pattern at the posterior of the cell (movie 2 in the electronic supplementary material shows the time-resolved animation). Qualitatively, they are very similar to the behaviour shown in figure 2*a*. In figure 3*b*, we provide illustrations of traction stress fields ($\boldsymbol{F}_{\mathrm{trac}}$) generated by our model cell during the same simulation

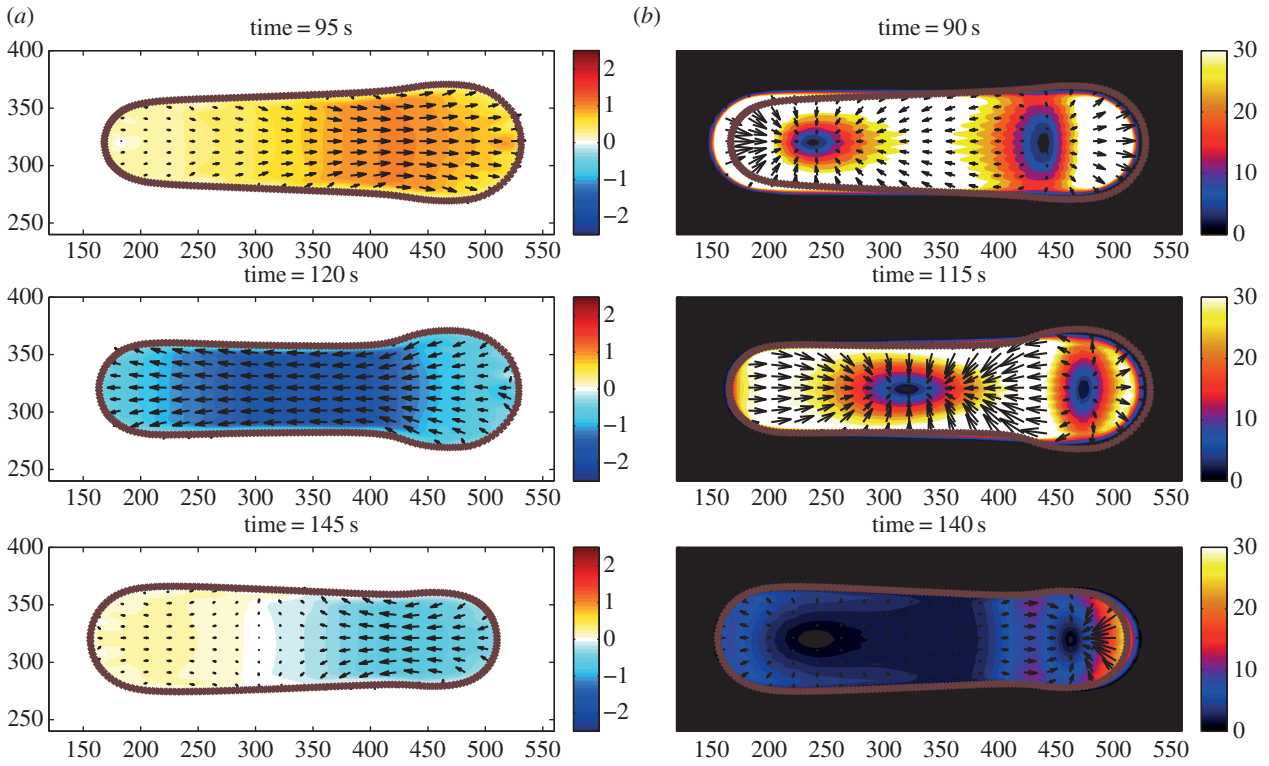

Figure 3. (*a*) Instantaneous intracellular flow computed in a model cell. Arrows indicate the direction of flow; the colourmap indicates the projection of flow velocity onto the cell axis ($\mu m\ s^{-1}$). (*b*) Instantaneous traction stresses computed in a model cell. Arrows indicate the direction of the stress field; the colourmap indicates the magnitude of the stress field (Pa). Again, all arrow fields are downsampled by a factor of 4 in each direction for visual clarity. (Online version in colour.)

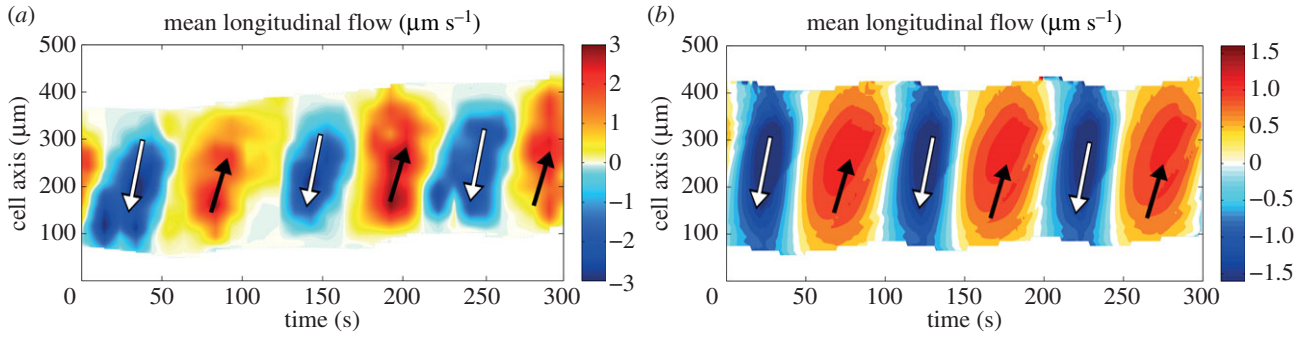

Figure 4. Kymographs of mean longitudinal flow $\bar{U}$. (*a*) Data recorded in migrating *Physarum*. (*b*) Values predicted by model simulation. Black arrows indicate flow directed forward. White arrows indicate regions of backward flow. (Online version in colour.)

shown in figure 3*a*. The time points shown are offset from those in figure 3*a* for a more direct comparison with experiments. The three panels show the forward propagation of a contractile locus of stress through the cell body, as well as a locus of expansive stress that exits the anterior of the cell before a weaker one emerges at the posterior (movie 3 in the electronic supplementary material shows the time-resolved animation). In this regard, the model again reproduces the qualitative behaviour observed in live *Physarum*.

To further analyse the flow patterns that we observe (or our model predicts), we generate kymographs of the measured (or calculated) longitudinal flow averaged over each lateral cross section of the cell

$$\bar{U}(x,t) = \frac{\int_{\Omega_c} \boldsymbol{u}_f \cdot \hat{x}\,\mathrm{d}y}{\int_{\Omega_c} \mathrm{d}y}, \tag{4.1}$$

where Ω_c denotes the interior of the cell, x is the longitudinal coordinate, y is the coordinate orthogonal to the longitudinal axis and $\hat{x}$ is the unit vector oriented towards the anterior of the cell. Similarly, we compare kymographs of the observed and measured traction stresses by defining

$$\bar{S}(x,t) = \frac{\int_{\Omega_c} \boldsymbol{F}_{\mathrm{trac}} \cdot \hat{x}\,\mathrm{d}y}{\int_{\Omega_c} \mathrm{d}y}, \tag{4.2}$$

which measures the average traction stress *in the direction of motion* at each cross section of the cell body.

Figure 4 shows experimental measurements of $\bar{U}$, together with results for the model cell. For both our experiments and simulations, we observe flows in good agreement with those reported previously [12]. A periodic pattern is clearly evident, where regions of forward and rearward flow are generated at the back of the cell, and quickly propagate towards the front in an approximately linear fashion. We refer to this pattern as a 'phase wave', and to its propagation speed as the 'phase velocity', c_ϕ. In previous experiments, this phase velocity was reported as $c_\phi = 12 \pm 1\ \mu m\ s^{-1}$ [12]. Here, we measure higher phase velocities, $c_\phi = 23.8 \pm 12.0\ \mu m\ s^{-1}$, across our

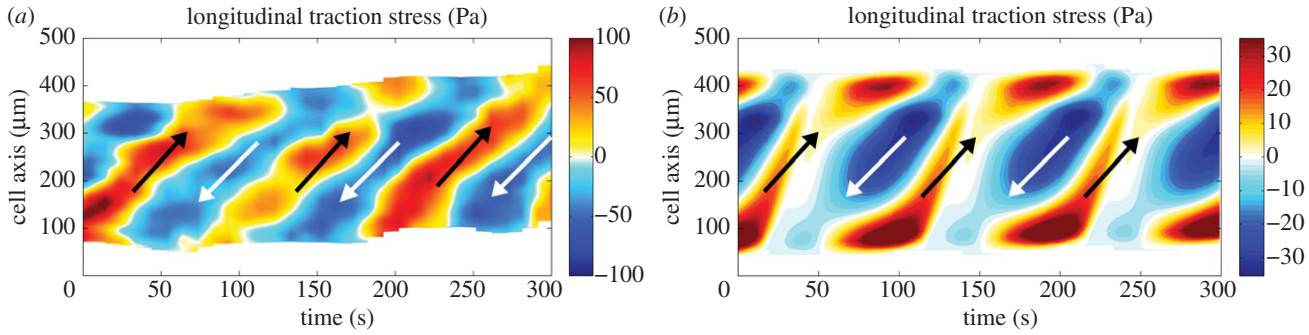

Figure 5. Kymographs of mean traction stress $\bar{S}$. (*a*) Data recorded in migrating *Physarum*. (*b*) Values predicted by model simulation. Black arrows indicate regions of stress directed forward. White arrows indicate stress directed backward. (Online version in colour.)

experiments, and our model predicts $24 \leq c_\phi \leq 38\,\mu\text{m s}^{-1}$ (see the electronic supplementary material).

Figure 5*a* shows a kymograph of traction stresses measured in the same experiment as figure 4*a* (with average cortical stresses removed). The data displayed are qualitatively representative of a large number of experiments. For comparison, figure 5*b* shows a traction stress kymograph for the model cell. In the kymographs, we see a distinct phase wave of adhesion stress similar to the flow pattern in figure 4. However, we note that, in both experiments and our model, the phase velocity of the flow patterns is approximately four times faster than that of the traction stress patterns. The numerically calculated traction kymograph reproduces the main features of the traction stresses observed in live *Physarum*. However, model and experiment do not agree in all respects. For example, for these parameters our model predicts that the maximal forward stresses occur at the anterior and posterior of the cell while this does not appear to be the case in experiments. Altering parameters changes this aspect of the model predictions, but may cause other disagreements with experiments. It is difficult to identify by visual inspection which adhesion parameters *most closely* reproduce the spatio-temporal dynamics of the adhesion stress observed in experiments. In §4.5, we develop a more quantitative analysis of the coordination of adhesion to compare experiments and calculations.

4.3. Role of flow

It is argued in [12] that the asymmetry in the motion of a fluid particle in such a flow pattern is directly responsible for the net displacement of the cell. Figure 6*a* illustrates this argument by showing particle paths in an idealized flow where regions of forward and backward flow propagate through the cell body. A particle translates forward and then backward with the same speed over one period of the wave. The particle is in a region of forward flow for more than half the period, resulting in net forward displacement. We define the asymmetry in the flow to be the ratio of the forward and backward displacement of such a particle path. Figure 6*b* shows the displacement of the centroid of a *Physarum* specimen. We define the centroid displacement asymmetry to be the ratio of the forward and backward displacements of the centroid over one period. In figure 6*c*, we plot the asymmetry in the flow as a function of the centroid displacement asymmetry, measured in our experiments. If the flux of mass due to the intracellular flow wave were solely responsible for the migration of the cell centre of mass, then the data in figure 6*c* would lie on the green dashed line with slope 1. However, this line is in fact a poor fit to the data, while the best linear fit (solid blue line) has a much lower slope of ≈0.16.

Examining figure 6*c* more closely reveals a critical phenomenon. We observe that 45% of the data points have a flow asymmetry less than unity, despite having a centroid asymmetry greater than unity (lower right quadrant in the figure). Thus, for a significant fraction of our observations the intracellular flow suggests a net *backward* translation of mass, even though the cell has moved forwards. For comparison, in figure 6*d*, we show flow kymographs from two cells. Cell A (marked with upward triangles in figure 6*c*) predominantly exhibits a flow asymmetry less than 1, while cell B (marked with downward triangles in figure 6*c*) predominantly exhibits a flow asymmetry greater than 1. Both exhibit similar phase velocities of the flow wave. While intracellular flow is likely to play a role in the migration of *Physarum*, our experiments (and model predictions in §4.4) indicate that intracellular flow kinematics alone cannot determine the migration of the cell.

4.4. Adhesion coordination and crawling speed

Figure 7 shows the centroid trajectories and flow kymographs for three cells generated with the model using different forms of adhesion coordination. Cell A uses a phase parameter of $\phi = 3\pi/2$ and an adhesion coefficient of $A = 100\epsilon$. Cell C uses the same adhesion coefficient, and a reversed phase parameter of $\phi = \pi/2$. Cell B was simulated with $\phi = 3\pi/2$ and adhesion coefficient $A = 0$. All three of these cells are driven with the same contraction pattern, but more importantly exhibit very similar flow patterns which are all consistent with both our experiments and experiments of others [9,12]. However, while cell A migrates forward consistent with experimental observations, cell B shows no net translation over the course of the simulation, and cell C migrates *backwards*. The implication is that, while hydrodynamic effects may generate stresses integral to motility, it is the coordination of the transmission of those stresses to the substrate that ultimately determines motility. Furthermore, from cell B we see that *coordinated* adhesion is critical to motility. A cell migrating using just the non-specific, uncoordinated adhesion (ϵ) fails to migrate.

For comparison, figure 6*b* provides a time course of the centre of a *Physarum* specimen migrating in the laboratory. Qualitatively, the predicted migration behaviour of model cell A closely matches that observed in our experiments. We see a distinct, periodic translation forward and backward, with a pronounced asymmetry to the two translations resulting in a net forward displacement of the cell. For the simulation shown, the net displacement of the model cell is approximately

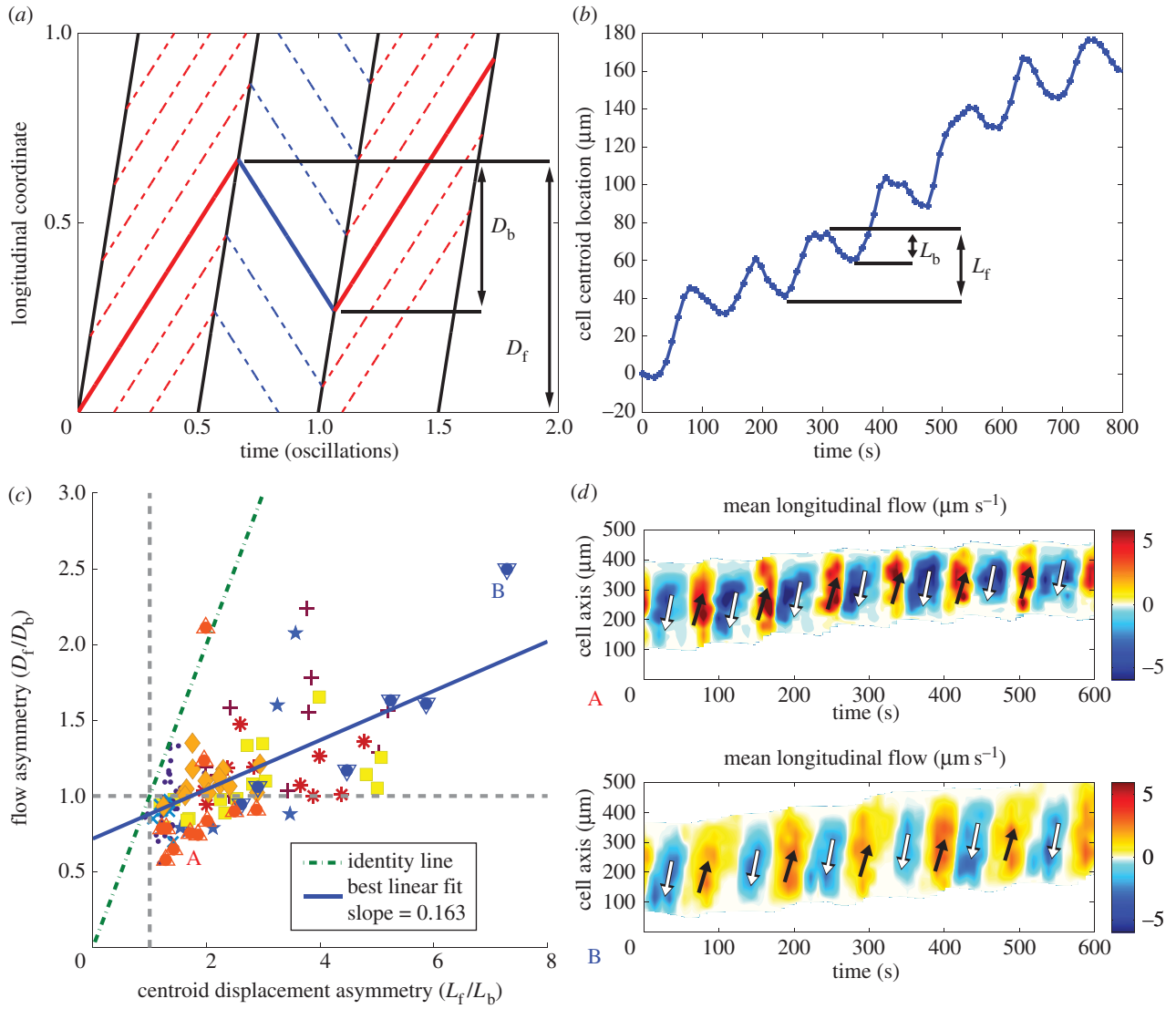

Figure 6. (*a*) An illustration of particle paths associated with a constant phase wave. The forward and backward particle displacements (D_f and D_b) are shown. Flow asymmetry is defined to be D_f/D_b. (*b*) A time series of the centroid of a migrating *Physarum*. The forward and backward centroid displacements (L_f and L_b) are shown. Centroid displacement asymmetry is defined to be L_f/L_b. (*c*) Experimentally measured values of flow and centroid displacement asymmetry over 118 periods (each datum point) and nine cells (distinguished by distinct markers). The best linear fit is shown in solid blue. The line $D_f/D_b = L_f/L_b$ is shown in dashed green for comparison. (*d*) Flow kymographs from the cells marked A (upward triangles) and B (downward triangles) in (*c*), illustrating flow asymmetry less than and greater than 1, respectively. (Online version in colour.)

6 μm per period, which is equivalent to an average migration velocity of $\approx 0.06\,\mu m\,s^{-1}$. In the laboratory, we measure *Physarum* migrating at speeds of $0.169 \pm 0.041\ \mu m\ s^{-1}$ across the 10 cells which exhibit peristaltic behaviour. Thus, our model predicts *Physarum* migration in reasonable agreement with experiments and suggests that coordination of adhesion and contraction is essential for efficient locomotion.

We now explore the speeds of migration predicted by the model as a function of adhesion strength and coordination. We perform simulations varying the phase parameter (ϕ) over eight equally spaced values from 0 to 2π, and the coefficient of adhesion (A) over six orders of magnitude. All parameter values give rise to similar periodic displacements (as shown in figure 7). However, depending on the phase and strength of adhesion, our model predicts various translation velocities and *directions* of migration (figure 8).

We observe that the migration velocity of the model cell is a non-monotonic function of adhesion coordination and strength. Indeed, the cell speed is maximal at moderate values of coordinated adhesion, while uncoordinated or strongly adherent cells display negligible migration. In the limit $A \ll \epsilon$, the coordinated adhesion is negligible compared with the uniform, uncoordinated adhesion and the cell cannot move directionally despite generating periodic cell shape changes (see cell B in figure 7). In the limit of strong adhesion $A \gg \epsilon$, the cell is effectively stuck to the substrate and cannot move even if this adhesion is highly coordinated. Experiments performed on highly adhesive substrates coated with collagen and the polycation poly-L-lysine [26] are qualitatively consistent with the model predictions. *Physarum* amoebae migrating on these sticky substrates adopt a tadpole shape, and create peristaltic contraction waves and intracellular streaming. However, they barely move (see the electronic supplementary material, movie 4).

As each simulation is driven with active contractions of the same amplitude and form, we may consider migration speed of the cell as a measure of efficiency. The cell translates most efficiently with an active adhesion coefficient of $A/\epsilon \sim 10-100$, and a coordination phase of $\phi \sim \pi - 3\pi/2$. Thus, the model predicts an optimal parameter regime in which to drive motility.

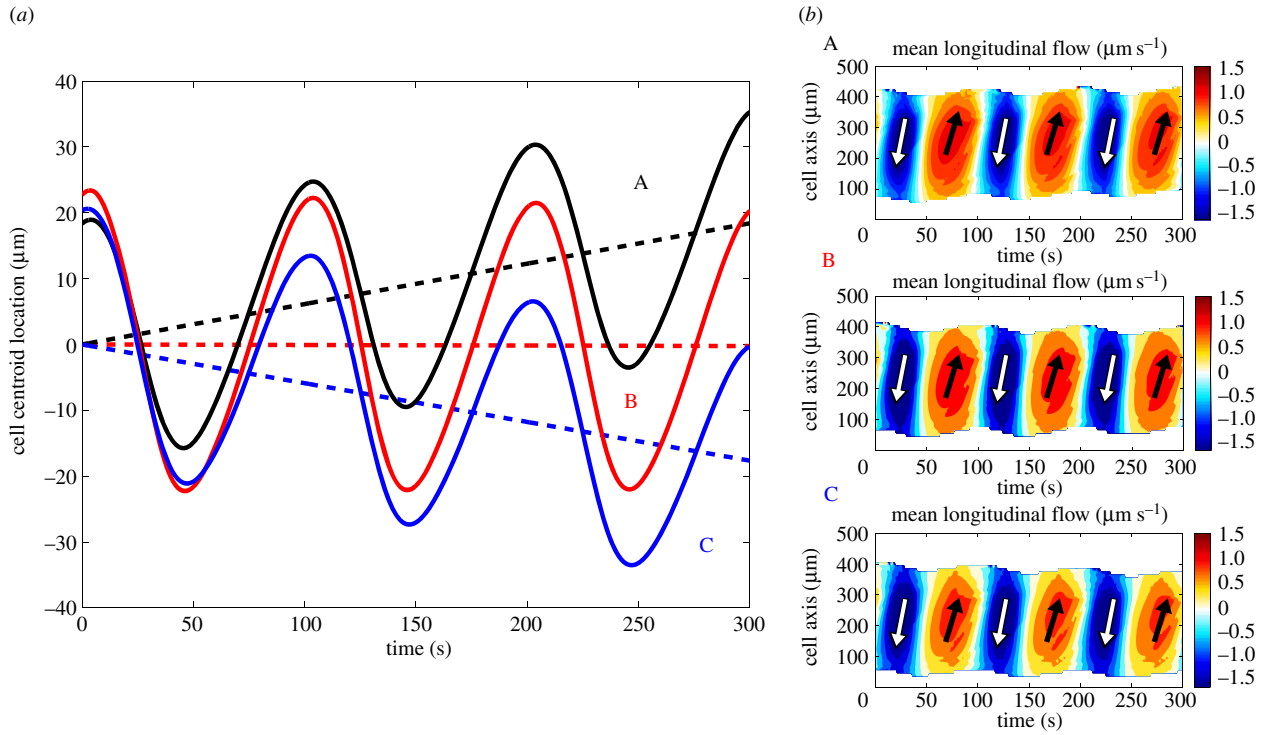

Figure 7. Numerically calculated time sequence of the cell centre is shown in (*a*). The solid lines indicate the centroids of individual cells, while the corresponding dashed lines indicate a best (least-squares) linear fit. Migration speeds reported are given by the slope of this fit. The flow kymographs of $\bar{U}$ for each cell are shown in (*b*). Black arrows indicate forward flow. White arrows indicate regions of backward flow. (Online version in colour.)

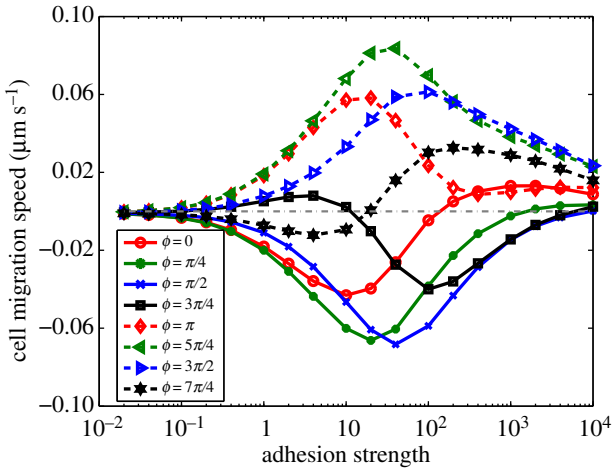

Figure 8. Average cell crawling speed as a function of adhesion coefficient and adhesion phase. The adhesion coefficient is reported in non-dimensional units [A/ε]. The dashed grey line indicates zero migration velocity. (Online version in colour.)

However, the parameters A and ϕ are not measurable in our experiments. In §4.5, we develop a quantitative measure of the relative timing of *flow* and *adhesion* within *Physarum*. This will be used to determine whether these model parameters are consistent with experiments.

4.5. Adhesion correlation

We examine the time evolution of the strain energy exerted by live migrating *Physarum* on their substrate (electronic supplementary material, equation S.5), and compare it with the evolution of the average intracellular flow velocity. The results show a distinct periodic pattern in both variables, with the flow wave preceding the adhesion wave by approximately a quarter period (figure 9*a*). This behaviour is robust across the nine reported experiments. To more precisely quantify this phase relationship between flow and adhesion energy, we calculate the cross correlation of flow and adhesion energy, as well as the autocorrelation of the flow wave (figure 9*b*). The distance between peaks of the autocorrelation function is interpreted as the period of the flow wave oscillation (T). The position of the first peak (restricted to times $t > 0$) of the cross-correlation function indicates the relative timing of the flow and energy waves (θ). The ratio θ/T defines the relative phase (between 0 and 1), which we measured to be 0.34 ± 0.07 in our experiments.

We perform the same analysis for the model simulations. Figure 10 shows the average intracellular velocity and strain energy within the model adhesions, as well as the auto and cross correlation of these two time sequences. The data shown are for a cell with $\phi = 3\pi/2$ and $A = 100\epsilon$, which is the same parameter set used for the forward moving cell in figure 7, as well as figures 4 and 5. For these parameters, the model reproduces accurately the observed phase relationship between flow and energy waves. We see a clear phase lag of approximately a quarter period.

Given the good agreement between model and experiments, we use the phase relationship between flow and energy to identify plausible adhesion parameters in the model. The results are shown in figure 11*a*, where we report the relative phase lag of the energy wave, in periods of the wave, for all simulations shown in figure 8. For reference, the relative phase observed in experiments (0.34 ± 0.07) is illustrated with the solid and dashed grey lines. The relative phase of adhesion energy appears to be highly sensitive to ϕ, and relatively insensitive to adhesion strength (beyond the range $A \approx \epsilon$). Values of ϕ in the range $3\pi/2$–2π (2π and 0 are equivalent) produce a relative timing which is consistent with experimental measurements. Of these parameter values, $\phi = 3\pi/2$ is the only one which produces migration in the forward direction regardless of the strength

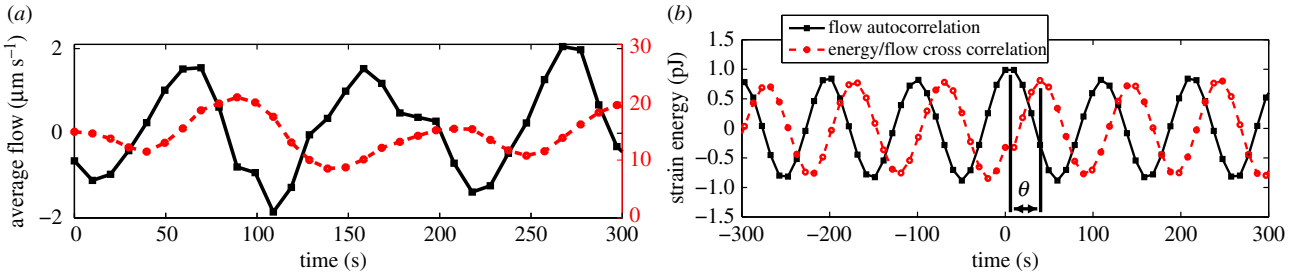

Figure 9. Experimentally measured flow (solid) and energy (dashed). (*a*) Average flow velocity within the cell interior, as well as total strain energy of adhesion as a function of time. (*b*) Auto and cross correlation of flow and energy, as well as the relative timing θ. (Online version in colour.)

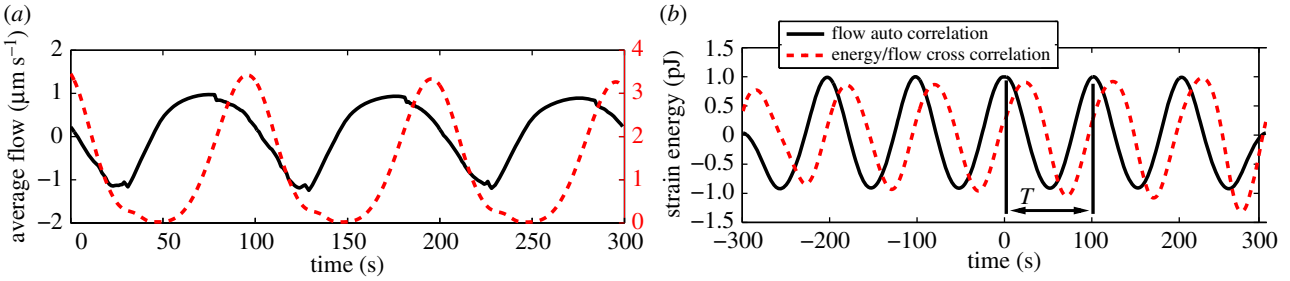

Figure 10. Numerically calculated flow (solid) and energy (dashed). (*a*) Average flow velocity within the cell interior, as well as total strain energy of adhesion as a function of time. (*b*) Auto and cross correlation of flow and energy, as well as the period *T*. (Online version in colour.)

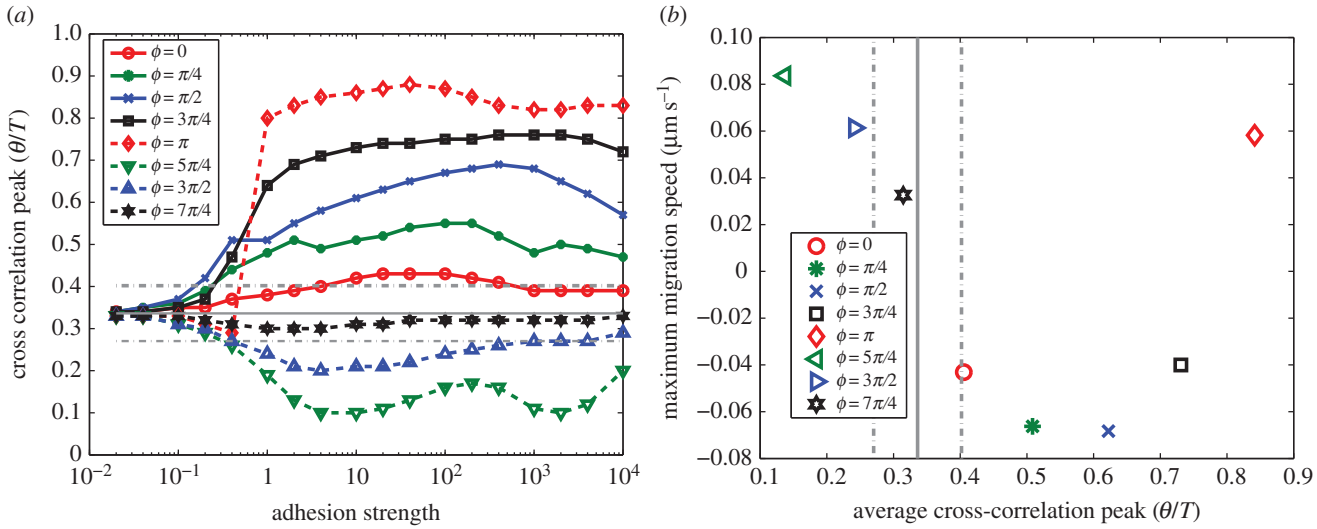

Figure 11. (*a*) Maximum cross correlation of elastic energy of adhesion and average cytoplasmic flow. The adhesion coefficient is reported in non-dimensional units $[A/\epsilon]$. Horizontal grey lines indicate the experimentally measured phase of 0.34 ± 0.07. (*b*) The average adhesion timing and maximum migration speed for each value of adhesion coordination ϕ. Vertical grey lines indicate the experimentally measured phase of 0.34 ± 0.07. (Online version in colour.)

of coordinated adhesion. For cells using $\phi = 3\pi/2$, the phase lag between flow and strain energy remains in the range 0.21–0.33 when varying the adhesion strength over six orders of magnitude. Specifically, in the case of highest migration velocity, we measure a phase lag of 0.25. In figure 11*b*, we show the average adhesion timing θ/T (calculated for all values $A > \epsilon$) and the maximum signed migration velocity for each value of the coordination parameter ϕ. Again, we see that, of the values of ϕ which are consistent with experiment, $\phi = 3\pi/2$ produces the maximum migration velocity.

4.6. Robustness

From the criteria discussed above, the spatio-temporal pattern of adhesion which is most consistent with experimental evidence corresponds to a phase lag of $\phi \approx 3\pi/2$ and a strength of $A \approx 100\epsilon$. Furthermore, these parameters predict nearly optimal migration velocity within the constraints of the model. It is noteworthy that this optimal migration velocity is not sensitive to the strength of adhesion. Returning to figure 8, we see that the model predicts a migration velocity above 0.03 μm s^{-1} (approx. 50% of maximal) over more than *two decades* of adhesion strength. Thus far, our simulations consider only spatially uniform substrates. In relevant environments, the strength of adhesive interactions between the cell and substrate is not homogeneous, as numerous extracellular and intracellular factors may affect such interactions. Therefore, we modify our model to quantify the robustness of migration with respect to spatial variations in adhesion strength. We alter the model of cell adhesions to the substrate in order to

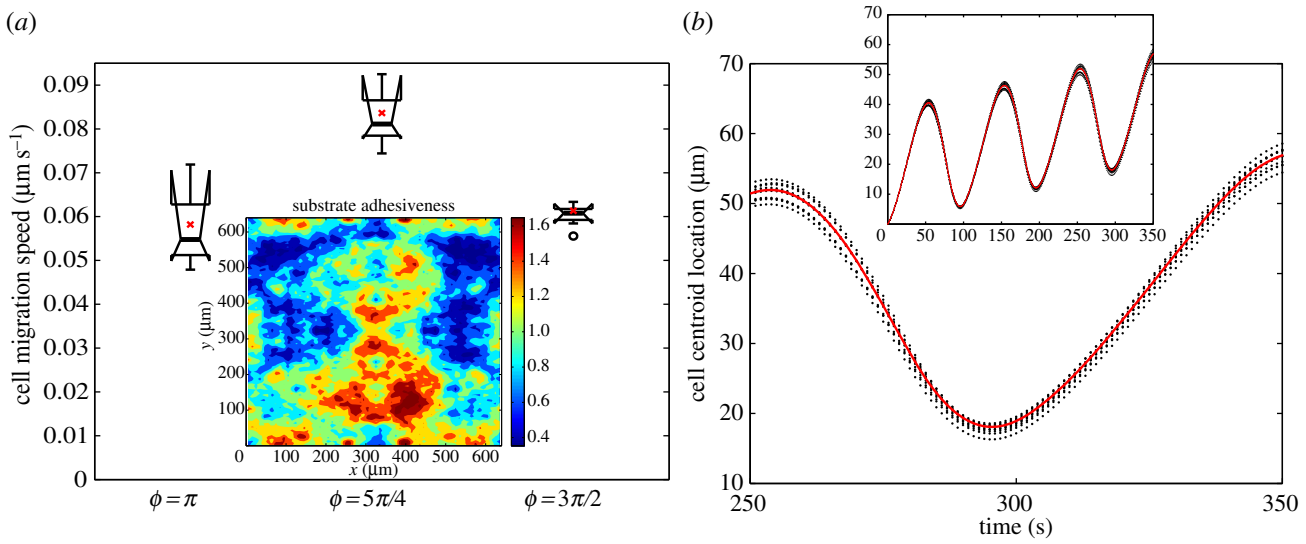

Figure 12. (*a*) Open circles indicate outliers in the dataset. Red crosses indicate the migration velocity calculated for a cell migrating across a homogeneous substrate. The inset shows a single randomly generated example of the spatial heterogeneity $g(x, y)$. (*b*) Dashed black lines indicate the time course of centroids of cells migrating across a random substrate. The solid red line indicates a cell migrating across a homogeneous substrate. $\phi = 3\pi/2$ in all cases. (Online version incolour.)

incorporate spatial heterogeneity. The existing form of adhesion (equation (3.7)) is replaced with

$$\zeta(x, t) = \frac{A}{2} g(x_{\text{lab}}, y_{\text{lab}}) \left(\cos\left(\frac{2\pi}{\ell_{\text{adh}}} x - \frac{2\pi}{T} t + \phi \right) + 1 \right) + \epsilon, \tag{4.3}$$

where $g(x_{\text{lab}}, y_{\text{lab}})$ is a randomly constructed function of fixed laboratory coordinates. By construction, this function has mean of $\mu_r = 1$ and standard deviation $\sigma_r = 0.34$ (for further details, see the electronic supplementary material). This has the effect of spatially modulating the strength with which the cell adheres to the substrate.

Using the randomly constructed function g to represent a heterogeneous substrate, we simulated cells migrating across 10 different substrates. We performed these simulations for the three values of ϕ which generically resulted in forward migration, and values of coordinated adhesion that results in the greatest migration velocity for each phase parameter. This means $\phi = \pi$, $5\pi/4$ and $3\pi/2$, with $A = 20\epsilon$, 40ϵ and 100ϵ, respectively. The results are summarized in the box plot of figure 12*a*. The spread of the data shows that migration speed is relatively insensitive to substrate heterogeneity for the considered values of ϕ. Note that the value $\phi = 3\pi/2$, which is most consistent with our live *Physarum* experiments, produces a substantially lower spread in migration speed, with half the data falling within $\pm 2.5\%$ of the median value. Thus, this spatio-temporal pattern of adhesion coordination is highly robust with respect to local variations in the strength of substrate adhesiveness.

Figure 12*b* shows the time evolution of the centroid of the 10 cells with random adhesion strength for $\phi = 3\pi/2$ (black), compared with the homogeneous substrate case (red). The inset shows the full time course, while the main panel shows just the final 100 s of migration. Over time, the location of the cells migrating across random substrates begins to deviate as random effects accumulate over time. However, these deviations are quite small compared with the scale of cell migration. This result indicates that, for the set of model parameters that reproduce the experimental measurements, the instantaneous speed of migration is remarkably insensitive to the spatial heterogeneity of the substrate throughout the whole oscillation period.

5. Discussion

Migrating amoeboid cells such as *Physarum* microplasmodia apply highly dynamic traction forces on their surroundings, leading to large shape changes and fast intracellular streaming flows. However, there is a paucity of simultaneous measurements of traction forces and intracellular streaming, which has made it difficult to develop mechanistic models that relate the forces driving amoeboid motion and the cellular deformations realizing this motion.

In this work, we combine simultaneous measurements of cytoplasmic flow and the traction stresses in migrating *Physarum* microplasmodia with detailed computational models of amoeboid migration that resolve the mechanics of cellular deformation and substrate adhesion. Our measurements reveal that *Physarum* amoebae move by creating travelling waves of contractile traction stresses with a well-defined period of approximately 100 s. The traction stress waves are similar in character to the previously observed waves of intracellular flow, but the flow waves consistently precede the stress waves by approximately one-quarter of a cycle. Inspired by this observation, we use our numerical model to investigate the consequences of migration using travelling waves of coordinated contraction and adhesion. Our investigations show that, by altering the timing of adhesion relative to the flow wave, the cell is able to migrate with different velocities and in different directions. These findings transform the previously established view that directional migration of *Physarum* amoebae is caused by the directionality of the flow waves [12].

By juxtaposing our modelling and experimental work, we have identified specific forms of generation and transmission of cellular forces which plausibly drive the migration of *Physarum* amoebae. Within the context of our adhesion model, our simulations and experiments reveal a distinct pattern of spatio-temporal coordination between contraction and adhesion which reproduces the experimentally measured cytoplasmic flows and traction stresses, and the scale of cell migration

speed. This coordination pattern consists of a phase lag of three-quarters of a cycle between adhesion and contraction ($\phi \approx 3\pi/2$). In addition to validating the model, this result provides insight into the underlying mechanism of amoeboid motility. The particular adhesion coordination pattern we highlight is extremely robust to perturbations in adhesive interactions with the extracellular environment, and results in nearly maximum migration speed within the context of the model. Interestingly, the adhesion coordination pattern that produces maximum migration speed ($\phi = 5\pi/4$) is less robust, possibly because it does not properly reproduce the relative timing of flow and traction stress. This insight into the potential compromises of different adhesion coordination would not have been possible through experimental investigations alone. Our model allows us a direct control over the coordination of adhesion that we are unable to control in a laboratory setting.

We note that our frictional adhesion model is rather independent of the precise nature of the cell–substrate interactions. While this model could be justified as a time-averaged effect of integrin-like molecular binding, this assumption is not necessary to arrive at the precise mathematical form that we use. Indeed, it is unclear how *Physarum* exerts stresses on its surroundings. Previous models have suggested that wave-like patterns of contraction may spontaneously arise from the coupling of the mechanics and chemistry of contraction in *Physarum* [20,21]. It is plausible that a similar mechanism may give rise to a wave-like modulation of the strength of adhesive interactions. Though it is unlikely that microplasmodia migrate using adhesive patterns as simple as our idealized wave of adhesion, our modelling assumptions are consistent with a variety of possible mechanisms. More experimental investigation into the specific nature of *Physarum*–substrate interaction is required.

While somewhat unique, the motility of *Physarum* microplasmodia shares fundamental characteristics with other forms of amoeboid migration. Rythmic cellular contractions of period approximately 100 s are known to drive the motion of neutrophil-like and *Dictyostelium* amoeboid cells [16,27]. In particular, while intracellular flow kinematics do not fully determine the motility of *Physarum*, our results suggest that cellular contractions are used to generate intracellular flows and cell locomotion. The use of pressure-driven flows of cytoplasm to generate translation has been widely observed in motile cells [2,27,28]. This is in contrast to cell types which use the polarity of actin filaments to generate polymerization-driven protrusions such as lamellapodia and filapodia [29]. Our experimental model does not generalize to this type of motility, but our modelling framework could be adapted to account for network polarity and polymerization stresses. Furthermore, the observed motility of *Physarum* is consistent with a model of cell–extracellular matrix interaction that does not require specific integrin-like binding molecules. It has been shown that neutrophils undergo amoeboid migration in three-dimensional environments in the absence of specific binding molecules [4]. This contributes to the growing notion that friction-mediated motility is biologically advantageous, as it is robust to geometric and mechanical changes in the extracellular matrix [3,28].

The form of amoeboid motility we observe in *Physarum* also shares many characteristics with locomotion in higher organisms. The travelling wave of contraction is similar to contraction patterns observed in migrating gastropods, annelids and *Dictyostelium* slugs. In both experimental and theoretical investigations of these organisms, it has been seen that the direction of contraction wave propagation is not the critical factor in determining migration direction. Rather, migration results from the timing of interactions between the organism and substrate [17,30]. As we have previously discussed, this same behaviour is observed in our model.

While *Physarum* locomotion shares this behaviour with various gastropods and annelids, we note that the amoeba moves on a vastly different scale from these organisms. The slugs observed in [17] ranged from 0.7 to 28 cm in length, while *Physarum* microplasmodia begin to migrate in this fashion after reaching a size of approximately 100 µm. This seems to indicate that a motility mechanism predicated on travelling waves of strain and appropriately timed adhesive interactions represents a robust design principle; one which is viable across length scales from cellular to macro. Indeed, the advantageous characteristics of *Physarum* have not gone unnoticed by the robotics community, where the organism has been the inspiration for biomimetic design [5,31].

Acknowledgements. We would like to thank T. Nakagaki and J. P. Rieu for their stimulating discussions, which contributed to this work. We would also like to acknowledge the input of Ruedi Meili and Juan C. Lasheras.

Funding statement. O.L.L. and R.D.G. were supported by NSF grant no. DMS-1160438 and NSF grant no. DMS-1226386. S.Z. and J.C.d.Á. were supported by NSF grant CBET-1055697 and National Institutes of Health grant no. 5R01GM084227-03.

References

1. Bray D. 2001 *Cell movements. From molecules to motility*. New York, NY: Garland.
2. Lämmermann T, Sixt M. 2009 Mechanical modes of 'amoeboid' cell migration. *Curr. Opin. Cell Biol.* **21**, 636–644. (doi:10.1016/j.ceb.2009.05.003)
3. Charras G, Paluch E. 2008 Blebs lead the way: how to migrate without lamellipodia. *Nat. Rev. Mol. Cell Biol.* **9**, 730–736. (doi:10.1038/nrm2453)
4. Lämmermann T *et al*. 2008 Rapid leukocyte migration by integrin-independent flowing and squeezing. *Nature* **453**, 51–55. (doi:10.1038/nature06887)
5. Piovanelli M, Fujie T, Mazzolai B, Beccai L. 2012 A bio-inspired approach towards the development of soft amoeboid microrobots. In *IEEE RAS EMBS Int. Conf. on Biomedical Robotics and Biomechatronics, Rome, Italy, 24–27 June 2012*, pp. 612–616. New York, NY: IEEE.
6. Allen RD, Pitts WR, Speir D, Brault J. 1963 Shuttle-streaming: synchronization with heat production in slime mold. *Science* **142**, 1485–1487. (doi:10.1126/science.142.3598.1485)
7. Ohl C, Stockem W. 1995 Distribution and function of myosin II as a main constituent of the microfilament system in *Physarum polycephalum*. *Eur. J. Protistol.* **31**, 208–222. (doi:10.1016/S0932-4739(11)80445-1)
8. Kukulies J, Brix K, Stockem W. 1987 Studies on microplasmodia of *Physarum polycephalum*. *Cell Tissue Res.* **250**, 125–134. (doi:10.1007/BF00214663)
9. Koya S, Ueda T. 1998 The onset of rhythmic streaming in the *Physarum* plasmodium. *ACH Mod. Chem.* **135**, 297–304.
10. Rieu J-P, Delanöe-Ayari H, Takagi S, Tanaka Y, Nakagaki T. 2015 Periodic traction in migrating large amoeba of *Physarum polycephalum*. *J. R. Soc. Interface* **12**, 20150099. (doi:10.1098/rsif.2015.0099)

11. Willert CE, Gharib M. 1991 Digital particle image velocimetry. *Exp. Fluids* **10**, 181–193. (doi:10.1007/BF00190388)
12. Matsumoto K, Takagi S, Nakagaki T. 2008 Locomotive mechanism of Physarum plasmodia based on spatiotemporal analysis of protoplasmic streaming. *Biophys. J.* **94**, 2492–2504. (doi:10.1529/biophysj.107.113050)
13. Brix K, Stockem W. 1987 Studies on microplasmodia of *Physarum polycephalum*. *Cell Biol. Int. Rep.* **11**, 529–536. (doi:10.1016/0309-1651(87)90015-4)
14. Dembo M, Wang YL. 1999 Stresses at the cell-to-substrate interface during locomotion of fibroblasts. *Biophys. J.* **76**, 2307–2316. (doi:10.1016/S0006-3495(99)77386-8)
15. Rieu J-P, Barentin C, Maeda Y, Sawada Y. 2005 Direct mechanical force measurements during the migration of *Dictyostelium* slugs using flexible substrata. *Biophys. J.* **89**, 3563–3576. (doi:10.1529/biophysj.104.056333)
16. Del Álamo JC, Meili R, Alonso-Latorre B, Rodriguez-Rodriguez J, Aliseda A, Firtel RA, Lasheras JC. 2007 Spatio-temporal analysis of eukaryotic cell motility by improved force cytometry. *Proc. Natl Acad. Sci. USA* **104**, 13 343–13 348. (doi:10.1073/pnas.0705815104)
17. Lai JH, Alamo JC, Rodríguez-Rodríguez J, Lasheras JC. 2010 The mechanics of the adhesive locomotion of terrestrial gastropods. *J. Exp. Biol.* **213**, 3920–3933. (doi:10.1242/jeb.046706)
18. Strychalski W, Guy RD. 2013 A computational model of bleb formation. *Math. Med. Biol.* **30**, 115–130. (doi:10.1093/imammb/dqr030)
19. Del Álamo JC, Meili R, Alvarez-Gonzalez B, Alonso-Latorre B, Bastounis E, Firtel R, Lasheras JC. 2013 Three-dimensional quantification of cellular traction forces and mechanosensing of thin substrata by Fourier traction force microscopy. *PLoS ONE* **8**, e69850. (doi:10.1371/journal.pone.0069850)
20. Radszuweit M, Alonso S, Engel H, Bär M. 2013 Intracellular mechanochemical waves in an active poroelastic model. *Phys. Rev. Lett.* **110**, 138102. (doi:10.1103/PhysRevLett.110.138102)
21. Radszuweit M, Engel H, Bär M. 2014 An active poroelastic model for mechanochemical patterns in protoplasmic droplets of *Physarum polycephalum*. *PLoS ONE* **9**, e99220. (doi:10.1371/journal.pone.0099220)
22. Strychalski W, Copos CA, Lewis OL, Guy RD. 2015 A poroelastic immersed boundary method with applications to cell biology. *J. Comput. Phys.* **282**, 77–97. (doi:10.1016/j.jcp.2014.10.004)
23. Hayase M, Maekawa A, Yubisui T, Minami Y. 2008 Properties, intracellular localization, and stage-specific expression of membrane-bound β-glucosidase, BglM1, from *Physarum polycephalum*. *Int. J. Biochem. Cell Biol.* **40**, 2141–2150. (doi:10.1016/j.biocel.2008.02.019)
24. Srinivasan M, Walcott S. 2009 Binding site models of friction due to the formation and rupture of bonds: state-function formalism, force-velocity relations, response to slip velocity transients, and slip stability. *Phys. Rev. E* **80**, 046124. (doi:10.1103/PhysRevE.80.046124)
25. Álvarez-González B, Meili R, Bastounis E, Firtel RA, Lasheras JC, Del Álamo JC. 2015 Three-dimensional balance of cortical tension and axial contractility enables fast amoeboid migration. *Biophys. J.* **108**, 821–832. (doi:10.1016/j.bpj.2014.11.3478)
26. Jay PY, Pham PA, Wong SA, Elson EL. 1995 A mechanical function of myosin II in cell motility. *J. Cell Sci.* **108**, 387–393.
27. Bastounis E, Meili R, Álvarez-González B, Francois J, Del Álamo JC, Firtel RA, Lasheras JC. 2014 Both contractile axial and lateral traction force dynamics drive amoeboid cell motility. *J. Cell Biol.* **204**, 1045–1061. (doi:10.1083/jcb.201307106)
28. Tozluoğlu M, Tournier AL, Jenkins RP, Hooper S, Bates PA, Sahai E. 2013 Matrix geometry determines optimal cancer cell migration strategy and modulates response to interventions. *Nat. Cell Biol.* **15**, 751–762. (doi:10.1038/ncb2775)
29. Blanchoin L, Boujemaa-Paterski R, Sykes C, Plastino J. 2014 Actin dynamics, architecture, and mechanics in cell motility. *Physiol. Rev.* **94**, 235–263. (doi:10.1152/physrev.00018.2013)
30. Tanaka Y, Ito K, Nakagaki T, Kobayashi R. 2012 Mechanics of peristaltic locomotion and role of anchoring. *J. R. Soc. Interface* **9**, 222–233. (doi:10.1098/rsif.2011.0339)
31. Umedachi T, Idei R, Ito K, Ishiguro A. 2013 True-slime-mould-inspired hydrostatically coupled oscillator system exhibiting versatile behaviours. *Bioinspir. Biomim.* **8**, 035001. (doi:10.1088/1748-3182/8/3/035001)